# Stability of sectored morphologies of polymer lamellae

C. Saichand and Yashodhan Hatwalne
*Raman Research Institute, C.V. Raman Avenue, Bangalore 560 080, India*

Murugappan Muthukumar*
*Department of Polymer Science and Engineering, University of Massachusetts, Amherst, Massachusetts 01003, USA*

(Received 6 September 2023; accepted 17 October 2023; published 22 November 2023)

When a solution of interpenetrating and entangled long flexible polymer chains is cooled to low enough temperatures, the chains crystallize into thin lamellae of nanoscopic thickness and microscopic lateral dimensions. Depending on the nature of the solvent and growth conditions, the lamellae exhibit several sectors that have differing growth kinetics and melting temperatures. Remarkably, these lamellae can spontaneously form tentlike morphology. The experimentally well-documented phenomenology of lamellar sectorization and tent formation has so far eluded a fundamental understanding of their origins. We present a theoretical model to explain this longstanding challenge and derive conditions for the relative stabilities of planar, sectored, and tent morphologies for polymer lamellae in terms of their elastic constants and interfacial tensions. While the present model offers an explanation of the origin of the spontaneous formation of sectored tentlike morphology as well as sectored planar morphology, in contrast to planar unsectored morphology, predictions are made for morphology transformations based on the materials properties of the polymeric lamellae.

DOI: 10.1103/PhysRevE.108.054501

## I. INTRODUCTION

Polymer crystals are fascinating because they are formed by long, entangled, and interpenetrating chains. There is a topological frustration that the polymer chains need to overcome for settling into crystalline order. The frustration arises from the highly entangled collection of interpenetrating, connected chains with long-ranged spatial and dynamic correlations before crystallization begins. The chains have large free-energy barriers to reorganize polymer conformations into the ordered states [1]. Interestingly, the chains overcome the barrier to form polymer crystals [2,3]. Because of the connectedness, polymer crystals are different from regular atomic and molecular crystals. In contrast to regular crystals in three dimensions, polymer crystals are not periodic in all three dimensions. The free energy of polymers, particularly the configurational entropy of the polymer chains, compels polymer crystals to form lamellae [4,5].

The adjacent-reentry fold model (proposed by Keller [6]) is widely accepted to explain the structure of lamellae through polymer chains. According to this model, parts of polymer chains form rigid stemlike structures attached to adjacent stems by flexible folds in the polymer. These stems offer crystalline order by arranging on a lattice [see Fig. 1(a)]. Depending on growth conditions, stems can align either along the lamellar normal or at an angle with respect to it [2,3,7]. The lamella also comprises flexible chains like cilia and hairlike microscopic structures. For example, the crystalline state of polyethylene (PE) lamellae is in base-centered orthorhombic symmetry. The stems are tilted with respect to lamella normal by $\sim 30^\circ$ [see Fig. 1(b)]. The stems are in the trans configuration, and the folds are mainly in the gauche configurations.

Crystallization from a solution containing sufficiently long and unentangled flexible polymer molecules is observed to form diverse morphologies of single lamellar crystallites such as flat sectors, hollow pyramids, disks, onionlike scrolls, and twisted morphologies [7–11]. The typical thickness of a single lamella is on the order of 10 nm and lateral dimensions of about micrometers or above. The size, shape, and regularity of the crystals depend on their growth conditions such as solvent, temperature, concentration, and rate of growth. For example, flat lozenge-shaped lamellae are formed when PE is crystallized from a mixture of tetrachloroethylene and p-xylene [3], and flat hexagonal-shaped lamellae are formed when polyoxymethylene is crystallized from bromobenzene [9].

Even though sectors and hollow pyramids (sometimes referred as tents; hereafter, we call them tents) are observed experimentally, few theoretical models are used to investigate them. A fascinating approach involving topological defects in the folds was developed by Alageshan *et al.* [12] to study the stability of the flat-sectored morphology of polymer crystals. We use concepts borrowed from liquid-crystal physics and the physics of crystalline membranes to study the flat-sector morphology in Ref. [12].

For the stability of tents, a natural question arises why deformed tents are favored when compared with planar structures such as flat sectors and flat uniform morphologies. In this paper, we address this question based on the energetics of polymer morphologies. We follow the same approach as in Ref. [12] to investigate the stability of tent and flat-sector

*muthu2346@gmail.com

 

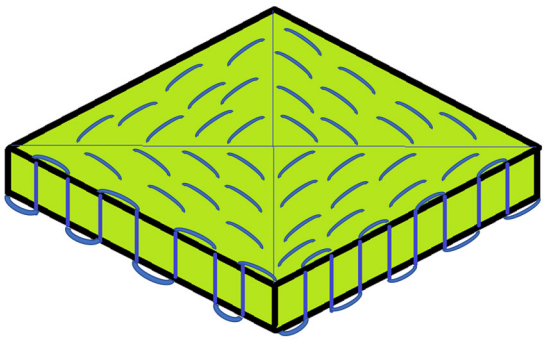

(a)

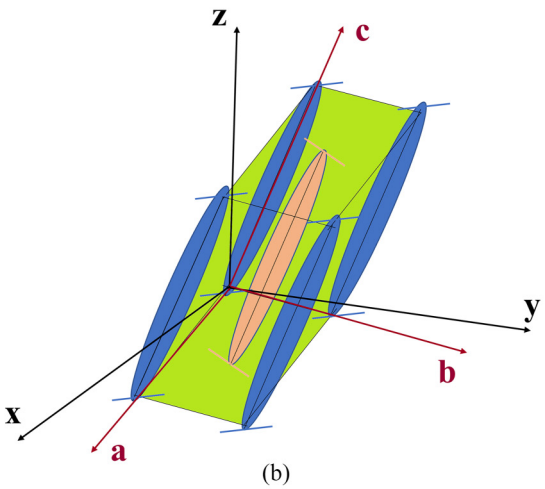


(b)

FIG. 1. (a) Cartoon of adjacent reentry model depicted in sectored lamella. The hairpinlike structures on the lamellar surface produce the fold field. (b) Schematic illustration of the unit cell of a crystalline polyethylene lamella. The unit cell has base-centered orthorhombic symmetry. Here, **a**, **b**, and **c** represent the crystal axes, and lamella are $xy$ plane, with lamellar normal along the $z$ axis. Note that the **c** axis of the unit cell is tilted with respect to the $z$ axis. Blue and orange shaded ellipsoids represent oriented stems formed by the all-trans configurations. Folds are not shown.

morphologies in polymer crystals. However in Ref. [12], the core energetics of the topological defect in the fold field of the flat sector is not mentioned explicitly. Therefore, we correctly account for this in the stability analysis of tent and flat-sector morphologies.

In this paper, we present a minimal model to study a spontaneous selection of tent morphology compared with flat-sector and uniform morphologies in polymer crystals. Using phenomenological theories, we evaluate the free energies corresponding to crystalline order and distortions in stem and fold fields of a single polymer lamella. The surface tension, line tensions (isotropic and anisotropic), and bending also contribute to the free energy of a given polymer morphology. As a result of the interplay between in-plane order, topological defects, and geometry, topological defects in the flexible crystalline [13] and hexatic [14] membranes buckle to reduce in-plane stresses. Interestingly, positive and negative defects of equal strength prefer locally positive (spherelike) and negative (saddlelike) Gaussian curvatures.

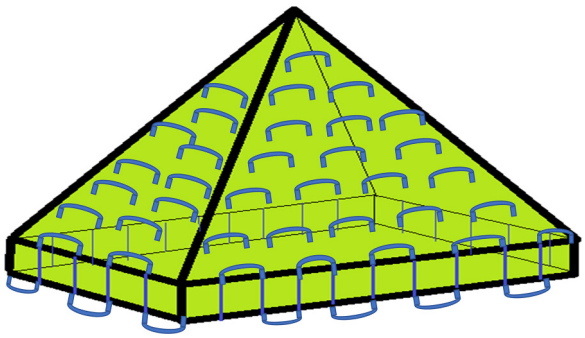

FIG. 2. Cartoon of a hollow tent morphology. Each face of the tent has a uniform fold configuration.

The key result of this paper is that we extend the buckling phenomenon to polymer crystalline lamellae and show that tents are buckled sectors (Fig. 2). The competition between the distortions in the fold, stem fields, and bending deformation determines the polymer configurations. The apex angle of the tent configuration is determined by the tilt of the polymer stems. Within the framework of the model, we study the stability analysis and obtain a morphology diagram indicating the stability of flat-uniform, flat-sector, and tent configurations over suitable parameters such as anisotropic line tension and elastic constants corresponding to folds, stems, and bending. In what follows, we give details of the model in Sec. II and present equilibrium equations and equilibrium configurations, respectively, in Secs. III and IV. The energetics of flat-uniform, flat-sector, and tent configuration are discussed in Sec. V. In Sec. VI, we discuss the results of the numerically obtained morphology diagram, followed by a concluding section.

## II. MODEL

For simplicity, we focus on structural and topological aspects of the flat sectors and tent configurations but do not address the detailed experimental conditions such as particular solvents, growth rate, and temperature. We treat the polymer configurations as mechanical and thermodynamical equilibrium structures. We also assume that the polymer lamella is a thin crystalline plate or membrane that uses continuum elastic theory (plate theory) [15].

Let $\mathbf{R}(\underline{\mathbf{x}})$ be the parameterization of a given two-dimensional (2D) polymer crystalline membrane embedded in three dimensions with the internal coordinates $\underline{\mathbf{x}} = (x^1, x^2)$. In general, a single polymer crystal has in-plane (i) crystalline order from polymer stems, (ii) tilt order of polymer stems, and (iii) orientational order from the fold field. The distortions in these in-plane orders play a significant role in the stability of polymer morphologies. For nonplanar morphologies, there are also bending deformations. Therefore, the competition between deformations in the underlying in-plane orders and bending of the lamella—thus, the total free energy of the system—dictates the stable configuration of the polymer lamellae. In this section, we discuss the phenomenological theories corresponding to the free energy of the polymer lamellae.

### A. Crystalline order: Hookean elasticity

The Hookean elastic free energy of the lamella depends on the symmetry of the point group that the underlying crystalline lattice possesses. For example, the orthorhombic symmetry of PE has nine independent elastic constants. To simplify the problem, we consider homogeneous and isotropic crystalline order, which has two independent elastic constants. The Hookean elastic free energy is given by [15,16]

$$F_u = \frac{Y}{2(1+\nu_P)} \int \left( u_{\mu\nu}^2 + \frac{\nu_P}{1-\nu_P} u_{\mu\mu}^2 \right) d\mathcal{A}, \tag{1}$$

where $Y$ and $\nu_P$ are 2D Young's modulus and Poisson's ratio, and the linearized strain tensor, by definition, $u_{\mu\nu} = \frac{1}{2}(\partial_\nu u_\mu + \partial_\mu u_\nu)$. Here, $\mathbf{u}(\underline{\mathbf{x}}) = \{u_1(\underline{\mathbf{x}}),\ u_2(\underline{\mathbf{x}})\}$ is the 2D displacement vector for the in-plane crystalline order, and $d\mathcal{A} = \sqrt{g} dx^1 dx^2$ is the area element with the metric $g$ and notation $\partial_\mu = \partial/\partial x^\mu$ for $\{\mu, \nu\} = \{1, 2\}$.

### B. Stem field

In addition to crystalline order from the stems, the polymer lamella acquires a tilt order from the stems which are tilted with respect to lamellar normal. The projection of stems onto the tangent plane of the lamella formulates the tilt order. Mathematically, the tilt order of the polymer stems is the unit vector field given by $\hat{\mathbf{s}} = \hat{\mathbf{c}} - (\hat{\mathbf{c}} \cdot \hat{\mathbf{N}})\hat{\mathbf{N}}$, where $\hat{\mathbf{c}}$ and $\hat{\mathbf{N}}$ are the axis of the stem and lamellar normal, respectively [17,18]. For a flat lamella with unit normal along the $z$ axis, the projected stem field simplifies to $\hat{\mathbf{s}} = \{s_x,\ s_y\}$ such that $s_x^2 + s_y^2 = 1$. The elastic free energy due to deformations in the stem field is given by [17–19]

$$F_s = \int \left[ \frac{\tilde{K}_1}{2} (\nabla \cdot \hat{\mathbf{s}})^2 + \frac{\tilde{K}_2}{2} (\nabla \times \hat{\mathbf{s}})^2 \right] d\mathcal{A}, \tag{2}$$

where $\tilde{K}_1$ and $\tilde{K}_2$ are the splay and bend elastic constants, respectively, for the stem field, and $\nabla$ is the covariant derivative.

### C. Fold field

The orientation of folds depends on the symmetry of the underlying crystalline order of the polymer lamella. For PE, there are two possible fold directions [see Fig. 3(a)]. Folds along these two directions have different energies. Moreover, in the ground state configuration, folds at the two fold surfaces are uniformly aligned. Thus, the ground state of a lamella has up-down symmetry. The fold direction is described by an apolar vector field $\hat{\mathbf{n}}_f$ with $-\hat{\mathbf{n}}_f \equiv \hat{\mathbf{n}}_f$ symmetry. For a flat lamella, the fold field is given by $\hat{\mathbf{n}}_f(x, y) = \{\cos\phi(x, y),\ \sin\phi(x, y)\}$, where orientational field $\phi(x, y)$ is the angle made by $\hat{\mathbf{n}}_f$ with respect to the $x$ axis. Because of up-down symmetry, $\phi$ is measured modulo $\pi$. On a curved surface, the angle $\phi(\underline{\mathbf{x}})$ is measured modulo $\pi$ with respect to a local orthonormal frame $[\hat{\mathbf{e}}_1(\underline{\mathbf{x}}), \hat{\mathbf{e}}_2(\underline{\mathbf{x}})]$.

Unlike square or perfect hexagonal shapes, the side lengths of each sector can, in general, be different. Typically, sectors come in lozenge and hexagonal shapes depending on underlying crystalline order and growth conditions [2,3,7]. To make calculations tractable, we consider square-shaped sectors. A square shape can be obtained if the two possible directions for the PE folds shown in Fig. 3 have the same energy. To do this,

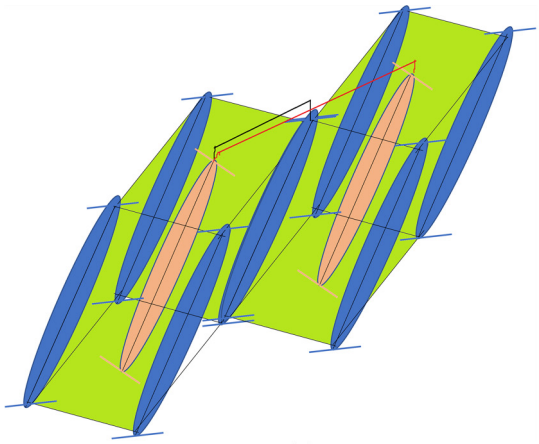

(a)

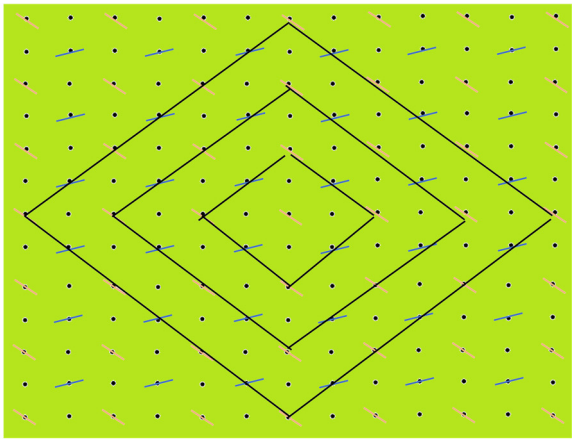

(b)

FIG. 3. Surface of the polyethylene (PE) lamella. (a) The black and red lines represent the two possible folds. Energetically, the black fold is favorable. (b) Viewed along the $c$ axis. Illustration of the lozenge-shaped, sectored lamella obtained by black lines.

we choose a potential that stabilizes square sectors as

$$V_\phi(\underline{\mathbf{x}}) = \frac{h_4}{4} \int \cos 4\phi(\underline{\mathbf{x}}) d\mathcal{A}, \tag{3}$$

where $h_4$ is the strength of the potential.

This potential has four equal minima at $\phi = \pi/4,\ 3\pi/4,\ 5\pi/4$, and $7\pi/4$ such that there are four equivalent ground states. Each ground state corresponds to a domain in the sector, and from one domain to another, the folds deform smoothly. In general, folds can deviate from the preferred direction, causing deformations in the fold field. To estimate the free energy cost, we use 2D nematic free energy as the lamella has up-down symmetry($-\hat{\mathbf{n}}_f \equiv \hat{\mathbf{n}}_f$), like the symmetry on nematic order. The corresponding Frank free energy is given by [19,20]

$$F_\phi = \int \left\{ \frac{K_1}{2} [\nabla \cdot \hat{\mathbf{n}}_f(\underline{\mathbf{x}})]^2 + \frac{K_2}{2} [\nabla \times \hat{\mathbf{n}}_f(\underline{\mathbf{x}})]^2 \right\} d\mathcal{A}, \tag{4}$$

where $K_1$ and $K_2$ are the splay and bend elastic constants for the fold field, respectively. In one constant approximation,

the free energy reduces to (for more details, see Appendix of Ref. [21])

$$F_\phi = \frac{1}{2}K_\phi \int g^{\mu\nu}(\partial_\mu\phi - A_\mu)(\partial_\nu\phi - A_\nu)d\mathcal{A}, \tag{5}$$

where $K_\phi$ is elastic constant, $g^{\mu\nu}$ is the inverse of metric tensor $g_{\mu\nu}$, and $A_\mu$ is the spin-connection term. By definition, $A_\mu = (\frac{1}{2})(\hat{\mathbf{e}}_1 \cdot \partial_\mu \hat{\mathbf{e}}_2 - \hat{\mathbf{e}}_2 \cdot \partial_\mu \hat{\mathbf{e}}_1)$.

### D. Coupling between crystalline order and folds

It is important to note that there is a coupling between the crystalline order ($u_{ij}$) and fold field ($\hat{\mathbf{n}}_f$) as shear deformations in crystalline order can change in fold orientation. Moreover, this coupling should be invariant under up-down symmetry (i.e., $-\hat{\mathbf{n}}_f \equiv \hat{\mathbf{n}}_f$). Keeping these considerations, the simplest coupling between $u_{ij}$ and $\hat{\mathbf{n}}_f$ is $[u_{ij} - (\frac{1}{2})\delta_{ij}u_{kk}]n_{f_i}n_{f_j}$ [22]. Note that this coupling is nonlinear because it involves two $\hat{\mathbf{n}}_f$ fields and one $\mathbf{u}$ field.

To be consistent with the harmonic approximation, we consider the de Gennes-type coupling used in nematic elastomers [23]. We use this coupling in the context of the crystalline and fold field ($\phi$ field) of polymer crystals. Rotations in the crystalline lattice are given by $\Theta = (\frac{1}{2})(\partial_x u_y - \partial_y u_x)$ [24]. It is a $z$ component of $(\frac{1}{2})\nabla \times \mathbf{u}$. For rigid rotations, changes in $\phi$ should match with $\Theta$, i.e., $\delta\Theta = \delta\phi$. The elastic free energy from nonuniform rotations in $\Theta$ and $\phi$ fields takes the form:

$$F_{\Theta\phi} = \frac{K_{\Theta\phi}}{2}\int (\delta\Theta - \delta\phi)^2 d\mathcal{A}, \tag{6}$$

where $K_{\Theta\phi}$ is a coupling constant. Note that $F_{\Theta\phi}$ is minimum for $\delta\Theta = \delta\phi$. This coupling ensures $\delta\Theta \approx \delta\phi$ for the crystalline lamella. Therefore, disclinations in the fold field would induce disclinations in crystalline order and vice versa. It is important to note that the elastic free energy of an isolated disclination in a flat crystalline membrane diverges as the square of the system size [13]. In contrast, the elastic free energy of an isolated disclination in nematic order diverges logarithmically with the system size [14]. In what follows, we ignore the coupling because of the prohibitively high elastic free-energy cost for disclinations in crystalline order [12].

### E. Bending: Helfrich free energy

Buckling involves the bending of polymer crystalline lamellae. For the free-energy cost corresponding to the bending of the polymer lamellae, we consider the Helfrich term [25]:

$$F_H = \frac{\kappa}{2}\int H^2 d\mathcal{A}, \tag{7}$$

where $\kappa$ is the bending rigidity of the lamella, and $H$ is the mean curvature of the buckled surface.

### F. Coupling between stems and curvature

In addition to the above bulk free-energy terms, there is an important coupling between polymer stems and curvature due to the bending of the polymer lamella. The bending of the polymer crystalline lamella can be achieved in two possible mechanisms (see Fig. 4). In the first mechanism, splaylike bending, the polymer stems undergo splay deformation to bend the lamella, whereas in the second mechanism, slidelike bending, the polymer stems are rearranged to be along the vertical direction via sliding mechanism without having splay deformation. The coupling between the polymer stem field ($\hat{\mathbf{s}}$) and curvature is given by [17,18]

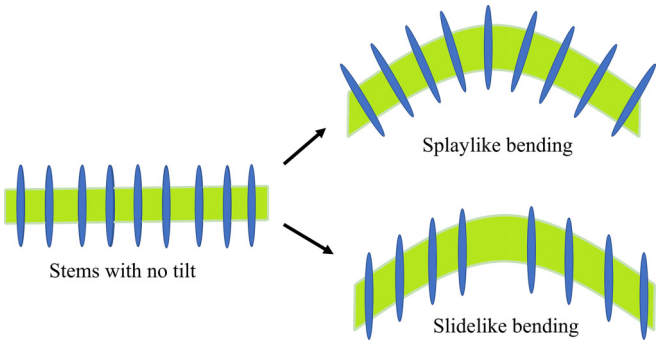


FIG. 4. Schematics of bending of the polymer crystalline lamella. Two types of bending: (i) splaylike bending in which polymer stems undergo splay deformation and (ii) slidelike bending in which the stems point along the vertical direction via the sliding mechanism.

$$F_{sH} = C\int (\nabla \cdot \hat{\mathbf{s}})\, H\, d\mathcal{A}, \tag{8}$$

where $C$ is the coupling constant. We note that the transformation: normal $(\hat{\mathbf{N}}) \rightarrow -\hat{\mathbf{N}}$ implies $\hat{\mathbf{s}} \rightarrow -\hat{\mathbf{s}}$ and $H \rightarrow -H$ such that the term $(\nabla \cdot \hat{\mathbf{s}})\, H$ remains invariant (bilayer symmetry).

### G. Surface and line tension energies

The polymer lamella has surface tension energy given by

$$F_\sigma = 2\tilde{\sigma}\int d\mathcal{A}, \tag{9}$$

where $\tilde{\sigma}$ is the surface tension. The factor 2 is for the upper and lower surfaces of the lamella. For simplicity, we use the notation $\sigma = 2\tilde{\sigma}$ to represent total surface tension.

For a polymer lamella with finite boundaries, the isotropic line tension free energy is given by

$$E_{\text{iso}} = \gamma \oint dl, \tag{10}$$

where $\gamma$ is isotropic line tension, and $dl$ is the length element on the boundary.

The anisotropic line tension generally prefers a particular angle between the fold field and outward normal to the boundary [26]. We model the anisotropic line tension as [26]

$$E_{\text{an}} = -\gamma_{\text{an}} \oint [\hat{n}_f \cdot (\cos\phi_0\, \hat{n}_b + \sin\phi_0\, \hat{t}_b)]^2\, dl, \tag{11}$$

where $\gamma_{\text{an}}$ is anisotropic line tension, $\phi_0$ is the preferred fold angle with boundary normal $\hat{n}_b$, and $\hat{t}_b$ is tangent to the boundary. To ensure $-\hat{\mathbf{n}}_f \equiv \hat{\mathbf{n}}_f$ symmetry, the term inside the integral is squared.

For the square sector, we choose $\phi_0 = \pi/2$, i.e., at the boundary, the fold field is aligned parallel to tangent $\hat{\mathbf{t}}_b$. With

this choice, the anisotropic line tension takes the form:

$$\begin{aligned} E_{\rm an} &= -\gamma_{\rm an} \oint (\hat{\mathbf{n}}_f \cdot \hat{\mathbf{t}}_b)^2 dl \\ &= -\gamma_{\rm an} \oint \cos^2(\phi - \phi_b) dl \\ &\equiv \gamma_{\rm an} \oint \sin^2(\phi - \phi_b) dl, \end{aligned} \tag{12}$$

where $\phi_b$ is the angle made by the tangent to the boundary with respect to local $\hat{\mathbf{e}}$ basis.

The total bulk free energy ($F$) of a buckled polymer crystalline lamella is

$$F = F_u + F_s + F_H + F_{sH} + F_\phi + V_\phi + F_\sigma. \tag{13}$$

With this background, we discuss the Euler-Lagrange equations of equilibrium for the buckled polymer lamellae.

## III. EQUILIBRIUM EQUATIONS

To obtain Euler-Lagrange equations of equilibrium, we minimize the total free energy ($F$) with respect to the stem field ($\hat{\mathbf{s}}$) and the fold field ($\phi$). The minimization with respect to $\hat{\mathbf{s}}$ gives

$$\frac{\delta F}{\delta \hat{\mathbf{s}}} = -\nabla[\tilde{K}_1(\nabla \cdot \hat{\mathbf{s}}) + CH] - \tilde{K}_2 \nabla \times \nabla \times \hat{\mathbf{s}} = 0. \tag{14}$$

The above vector equation is difficult to solve in general. Therefore, we consider a simple situation of curl-free stem configuration; that is $\nabla \times \hat{\mathbf{s}} = 0$. With this consideration, Eq. (14) reduces to $\tilde{K}_1(\nabla \cdot \hat{\mathbf{s}}) + CH = \text{const}$. Without loss of generality, we take const. $= 0$. Thus, the simplified equilibrium equation takes the form:

$$\nabla \cdot \hat{\mathbf{s}} = -\frac{C}{\tilde{K}_1} H. \tag{15}$$

After substituting the condition Eq. (15) into the total free-energy expression [Eq. (13)], we get the modified total free energy ($F$) as

$$F = F_u + F_\phi + V_\phi + \frac{1}{2}\kappa_{ef} \int H^2 d\mathcal{A}, \tag{16}$$

where the effective bending rigidity $\kappa_{ef} = \kappa - (C^2/\tilde{K}_1)$. We note that the effect of coupling between polymer stems and curvature reduces the bending rigidity.

The $\phi$ equation corresponding to the equilibrium fold field on the surface is given by

$$\frac{\delta F}{\delta \phi} = -K_\phi \nabla \cdot (\boldsymbol{\partial}\phi - \mathbf{A}) - h_4 \sin(4\phi) = 0, \tag{17}$$

where $\nabla\cdot$ represents covariant divergence. Note that the equation is a nonlinear partial differential equation in $\phi$ because of the $\sin(4\phi)$ term. These types of equations are known as sine-Gordon equations [16]. The one-dimensional solution to the sine-Gordon equation gives a wall or soliton solution.

Minimization of $F$ with respect to displacement vector $\mathbf{u}$ gives

$$\frac{\delta F}{\delta u^\mu} = \nabla_\nu \sigma_{\mu\nu} = 0, \tag{18}$$

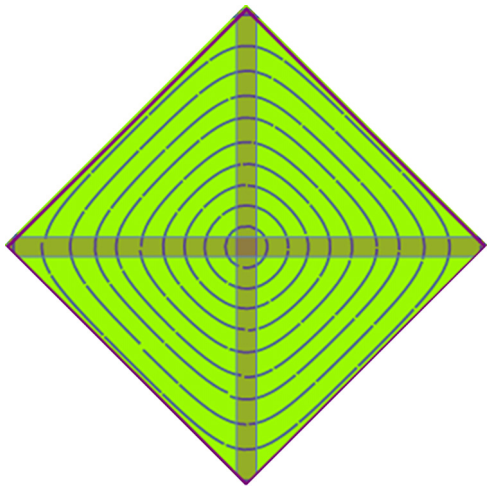

FIG. 5. Square sector: Texture of fold field obtained from the exact solution $\phi_s(x, y)$. Two shaded lines represent the soliton-type walls of wall width $w$. The fold field follows streamlines of $+1$ disclination, and the disclination core is located at the center of the square.

where the linearized stress tensor

$$\sigma_{\mu\nu} = \frac{Y}{1+\nu_P}\left(u_{\mu\nu} + \frac{\nu_P}{1-\nu_P} u_{\beta\beta}\delta_{\mu\nu}\right).$$

The general procedure for obtaining the equilibrium shape is to perform covariant minimization of the free energy ($F$) with respect to shape. However, the shape equation will be nonlinear and difficult to solve for general surfaces. For the tent surface, we use the ansatz solution discussed in the next section.

## IV. EQUILIBRIUM CONFIGURATIONS

In this paper, we investigate three basic morphologies of polymer crystals, namely, flat-uniform, flat-sector, and tent configurations. For a flat lamella, we can assign a fixed coordinate system such as $x$-$y$ axes to measure fold field $\phi$. Thus, the spin connection terms are zero [see Eq. (5)]. The $\phi$ equation reduces to

$$K_\phi\left(\partial_x^2\phi + \partial_y^2\phi\right) + h_4 \sin(4\phi) = 0. \tag{19}$$

A trivial, uniform solution to the above equation corresponds to one of the four minima. For example, we take the solution:

$$\phi^{(\rm Uni)} = \frac{\pi}{4}. \tag{20}$$

The nontrivial, soliton-type solution to Eq. (19) is [12]

$$\phi_s(x, y) = \arctan\left[\frac{\tanh(y/w)}{\tanh(x/w)}\right] - \frac{\pi}{2}, \tag{21}$$

where the length scale $w = \sqrt{K_\phi/h_4}$. Subtraction of $\pi/2$ in the solution ensures that the boundary condition that the fold field $\hat{\mathbf{n}}_f$ is parallel to the tangent to the boundary ($\hat{\mathbf{t}}_b$). The streamlines of the fold field in the square sector are depicted in Fig. 5. We note that the streamlines form a $+1$ disclination in the fold field with two intersecting walls, of wall width $w$

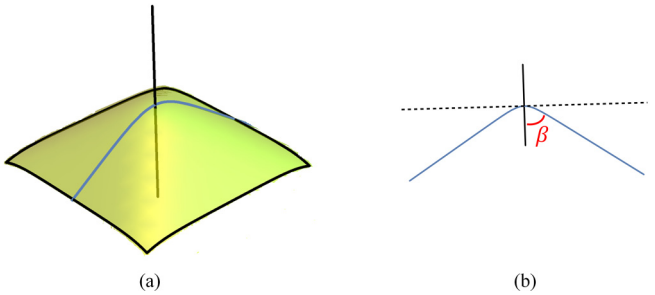


FIG. 6. (a) A hollow pyramid (tent) surface: A plot of the height function $h(x, y)$. The vertical black and blue lines represent the axis and faces of the tent surface, respectively. (b) Schematics of apex angle $(2\beta)$: By definition, the angle between the axis and face of the tent is $\beta$. The asymptotic slope of the tent face (blue line) is $\tan(\pi/2 + \beta)$.

each, along $x$ and $y$ axes, the point of intersection being the core of the disclination.

### A. Tent surface as an ansatz for shape equation

As mentioned in the previous section, we surmise the height function based on symmetries of the flat squared sector as that of a hollow pyramid (tent configuration). For that, we consider the parameterization of the surface (Monge representation) as $\mathbf{R}(x, y) = \{x, y, h(x, y)\}$, where $h(x, y)$ is the height function. With this representation, we get the metric $g = 1 + (\nabla_{xy} h)^2$, where $(\nabla_{xy} h)^2 = (\partial_x h)^2 + (\partial_y h)^2$. The ansatz height function corresponding to the tent surface is given by [see Fig. 6(a)]

$$h(x, y) = -a \ln\left(\cosh\left[\frac{x}{w}\right]\cosh\left[\frac{y}{w}\right]\right), \tag{22}$$

where parameter $a$ is the slope of the tent and the wall width of the flat sector $w = \sqrt{(K_\phi/h_4)}$. We note that the projection of the edges of the tent is along the $x$ and $y$ axes, respectively, and each quadrant represents the projected plane of the tent face. The asymptotic slope of the tent face is $\lim_{x\to\infty} dh(x, x)/dx = -2a/w$. If the apex angle of the hollow pyramid (tent) is $2\beta$, the slope is given by [see Fig. 6(b)]

$$-\frac{2a}{w} = \tan\left(\frac{\pi}{2} + \beta\right). \tag{23}$$

The buckling of the flat sector into a tent configuration involves the rearrangement of polymer stems. An illustration of polymer stems in tent configuration is shown in Fig. 7. We believe that the slidinglike bending of the polymer lamella is favorable. From the geometrical arguments, we can relate the tilt angle $(\theta)$ of the stem and apex angle $(2\beta)$ of the tent as follows (see Fig. 7):

$$\theta + \beta = \frac{\pi}{2}. \tag{24}$$

After substituting it into the slope formula [Eq. (23)], we get a relation between the parameter $a$ and the tilt angle as follows:

$$A_w = \frac{a}{w} = \frac{1}{2}\tan(\theta). \tag{25}$$

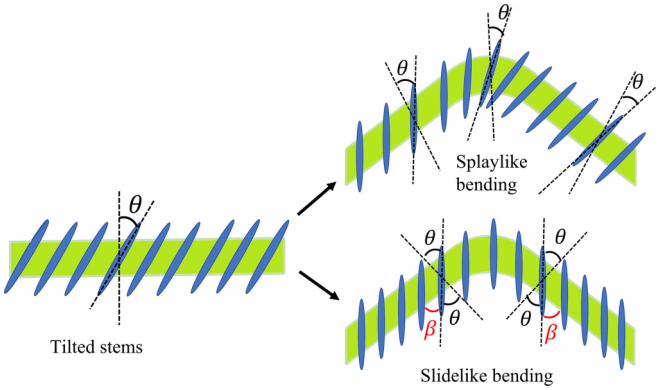


FIG. 7. Cartoon of buckling of polymer lamella with tilted stem into tent configuration.

Thus, the tilt angle of the stems determines the geometry of the tent surface.

For the equilibrium fold configuration on the tent surface $h(x, y)$, we need to solve Eq. (17) with the Monge approximation, i.e., $-K_\phi(\nabla^2_{xy}\phi - \nabla_{xy}\cdot\mathbf{A}) - h_4 \sin(4\phi) = 0$. We note the term $\nabla_{xy}\cdot\mathbf{A}$ is nonlinear in the height field $(h)$, and it is difficult to solve the equation analytically (see Appendix A for more details). Within the linear regime of the height field, we neglect the $\nabla_{xy}\cdot\mathbf{A}$ term. Then the $\phi$ equation reduces to that of the flat case [Eq. (19)], and $\phi_s$ is an exact solution. Therefore, we use $\phi_s$ as the equilibrium fold field on the tent surface by ignoring the contributions coming from the spin connection. This assumption is valid for $a \ll w$. Thus, we restrict ourselves to tent surfaces that are almost flat.

The cartoon of $\phi_s$ on the tent surface is shown in Fig. 8(a). We note that the disclination core coincides with the tent apex, each tent face has a uniform fold field, and the adjacent face is connected by a soliton-type wall in the fold field.

## V. ENERGETICS

To study the stability analysis, we compare the total free energies of flat-uniform, flat-sector, and tent configurations (Fig. 8). Throughout the calculations, we assume that the underlying crystalline order is the same for the three configurations considered. Thus, the Hookean elastic energy for the crystalline order in the three configurations remains constant. We also choose the surface areas of all three configurations as the same such that surface tension effects do not play a major role in stability. Let $l$ and $l_T$ be the side length of the flat sector (and uniform configuration) and the base length of the hollow pyramid (tent), respectively. The surface area of tent $\mathcal{A}_{\text{tent}} = \iint \sqrt{g}\, dx\, dy$. Upon equating areas of the flat sector and tent surface, we get the relation between $l$ and $l_T$ as

$$L = \sqrt{\mathcal{A}_{\text{tent}}}$$
$$L(A_w, L_T), \tag{26}$$

where $L = l/w$ and $L_T = l_T/w$.

Since the fold field is uniform, $F_\phi = 0$. Contribution from the potential is given by

$$V_\phi^{(\text{Uni})} = -\frac{h_4}{4} l^2, \tag{27}$$


(a) (b) (c)

FIG. 8. Schematics of the fold field. (a) On the tent surface (an exaggerated height field). Note the tent edges match with soliton-type walls in the fold field. The base length of the tent, in $w$ units, is $L_T$. The black square represents the core with side length $\zeta$ (in $w$ units). (b) For the flat sector of side length $L$ (in $w$ units). (c) For flat uniform configuration.

where the superscript (Uni) indicates the uniform configuration. The isotropic and anisotropic tensions take the form:

$$E_{\rm iso} = 4\gamma l,$$
$$E_{\rm an}^{\rm (Uni)} = 2\,\gamma_{\rm an} l. \tag{28}$$

We note that surface and line tensions are the same for the square sector of side length $l$; thus, we omit the superscript (Uni). The factor 4 in $E_{\rm iso}$ is due to four sides of the boundary, and for $E_{\rm an}^{\rm (Uni)}$, only two sides of the boundary follow the boundary condition, leaving out free-energy cost for the remaining two sides.

For mathematical simplifications, we define dimensionless fold free energy as

$$\mathscr{E}_T^{\rm (Uni)} = \frac{F_\phi + V_\phi + E_{\rm an} + E_{\rm iso}}{K_\phi}$$
$$\equiv \mathscr{E}_T^{\rm (Uni)}[\Gamma_{\rm iso}, \Gamma, L(A_w, L_T)], \tag{29}$$

where dimensionless side length $L = l/w$ and line tension parameters $\Gamma_{\rm iso} = (\gamma w)/K_\phi$, $\Gamma = (\gamma_{\rm an} w)/K_\phi$. Recall that wall width $w = \sqrt{K_\phi/h_4}$.

To calculate the energetics of sectors, we consider a square sectored lamella with side length $l$ (the same as for the uniform case) in the $x$-$y$ plane such that the walls coincide with the coordinate axes (see Fig. 5). We bear in mind that the fold field has a point disclination at the center, i.e., the origin. Thus, we need to use cutoffs for calculating $F_\phi$ and $V_\phi$ to avoid the singularities arising from the core of the disclination. Following the symmetry of the square-shaped lamella, we choose a square-shaped core with side length $\xi$ [see Fig. 8(b)]. Therefore, the core area is $\xi^2$.

Substituting the exact solution for $\phi$ [Eq. (21)] into $F_\phi$ with the appropriate core gives the elastic free-energy cost due to deformations in the fold field. However, the integrals are not analytically tractable. We use a numerical approach to calculate the total free energy (see Appendix B for more details). The dimensionless total energy of the square sector is given by

$$\mathscr{E}_T^{\rm (Sec)} = \frac{F_\phi + V_\phi + E_{\rm an} + E_{\rm iso}}{K_\phi}$$
$$\equiv \mathscr{E}_T^{\rm (Sec)}[\zeta, L(A_w, L_T), \Gamma_{\rm iso}, \Gamma], \tag{30}$$

where the superscript (Sec) indicates the sector configuration and dimensionless core size $\zeta = \xi/w$.

For tent energetics, we note that the fold field has a disclination at the apex. Thus, we use cutoffs for calculating $F_\phi$ and $V_\phi$ to avoid the singularities arising from the disclination. Following the symmetry of the square sector, we choose a square-shaped core with side length $\xi$ [see Fig. 8(a)]. As the integrals in free-energy calculations are analytically not solvable, we use a numerical approach (see Appendix B for more details). The total free energy of the tent configuration in $K_\phi$ is given by

$$\mathscr{E}_T^{\rm (Tent)} = \frac{F_\phi + V_\phi + F_H + E_{\rm an} + E_{\rm iso}}{K_\phi}$$
$$\equiv \mathscr{E}_T^{\rm (Tent)}(\zeta, A_w, L_T, \Gamma_{\rm iso}, \Gamma, \kappa_d), \tag{31}$$

where dimensionless bending rigidity $\kappa_d = \kappa_{ef}/(4K_\phi)$.

## VI. RESULTS: A MORPHOLOGY DIAGRAM

In this section, we obtain morphology diagrams indicating the stability of flat-uniform, sector, and tent configurations. Since the total energy of each configuration is a function of multiple dimensionless parameters $\{\Gamma_{\rm iso}, \Gamma, \kappa_d$ and $\zeta\}$, the morphology diagrams are complicated to represent in one plot. So we follow the procedure described below.

We numerically calculate $\mathscr{E}_T^{\rm (Uni)}$, $\mathscr{E}_T^{\rm (Sec)}$, and $\mathscr{E}_T^{\rm (Tent)}$ for a given core size $\zeta$, $A_w$ for varying values of $\kappa_d$, $L_T$, $\Gamma_{\rm iso}$, and $\Gamma$. For fixed $\zeta$, we find morphology boundaries by equating the total energy of each configuration. For example, the flat sector–tent boundary is obtained by equating the total energies of the sector and tent. The surface plots of morphology diagrams for PE crystal are shown in Fig. 9. For PE crystal, the tilt angle $\theta \simeq \pi/6$; thus, $A_w \simeq (\frac{1}{2})\tan(\pi/6) = 1/(2\sqrt{3})$. In our calculations, we choose $\zeta = 0.01$ (the same core size as the sector). For better representation, we give the line plots by intersecting the surface plots with constant $\kappa_d$ planes. The corresponding morphology diagrams as a function of $\Gamma_{\rm iso}$ and $L_T$ for various $\kappa_d$ and $\Gamma$ given in Fig. 10.

From the morphology diagram (Fig. 10), it is clear that the tent configuration is stable for small bending rigidity ($\kappa_d$), large line tension ($\Gamma_{\rm iso}$, $\Gamma$) values, and sizes ($L_T$). The sector configuration is favorable for large $\kappa_d$ and $L_T$ and moderate values of $\{\Gamma_{\rm iso}, \Gamma\}$. The results can be understood easily: As

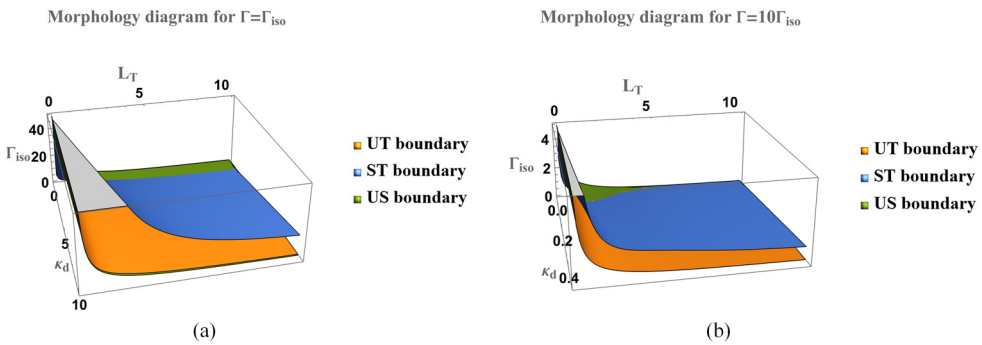


FIG. 9. Surface plots: The boundaries of two morphologies plotted as a function of parameters corresponding to isotropic line tension ($\Gamma_{\rm iso}$), base length of the tent ($L_T$), and bending rigidity ($\kappa_d$) for fixed anisotropic line tension parameter ($\Gamma$). Here, the abbreviations UT, ST, and US denote the uniform tent, sector tent, and uniform sector boundaries. For understanding the stability, consider the UT boundary. We note that, below (above) the UT boundary surface, uniform configuration (tent configuration) is favorable. The exact stability range of each configuration is obtained by considering all the boundaries. For example, the sector is stable in the region between blue and orange surfaces. Gray also represents the stable sector region. It is an artifact caused by the restriction of $\Gamma_{\rm iso}$ values, like an intersection of $\Gamma_{\rm iso}$ = const. planes.

the line tension parameters increase, trapping of disclination in the fold field becomes stronger, which stabilizes the sector formation. The lower bending rigidity favors the sector buckling into the tent configuration. We note that, depending on the parameter values, the tent configuration can be obtained directly from the flat-uniform configuration without forming sector configuration [see Figs. 10(a) and 10(c)]. However, the sector configuration is stabilized for a different set of parameters and becomes an intermediate configuration in the transition from flat-uniform to tent configuration [see Figs. 10(b) and 10(d)].

We also investigate critical bending rigidity ($\kappa_d^*$), the minimum value of bending rigidity required for the flat sector to buckle into the tent. The surface plot of critical bending rigidity as a function of $\Gamma$ and $L_T$ for $\Gamma_{\rm iso} = 1$ is shown in Fig. 11(a). The line plots corresponding to the surface plots with the intersection of $\Gamma$ = const. planes and $L_T$ = const. are given in Figs. 11(b) and 11(c), respectively. Interestingly, for large side lengths of the tent, the critical bending rigidity saturates for anisotropic line tension values.

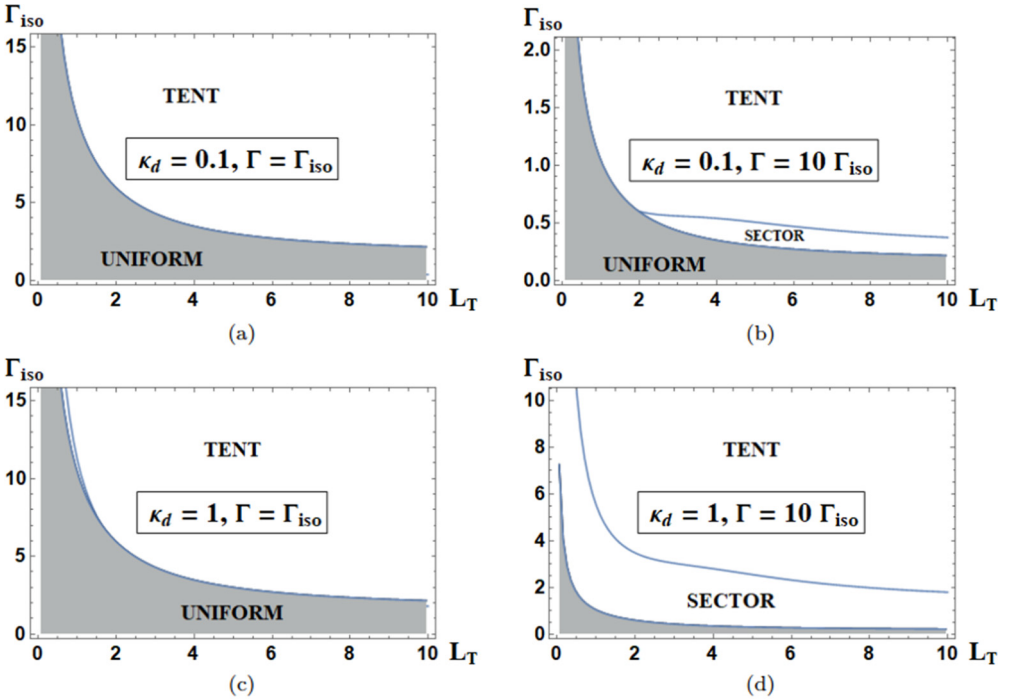


FIG. 10. The morphology diagram: Figures indicating the stability range of the tent, the flat sector and the flat uniform. They are plotted as a function of parameters corresponding to isotropic line tension ($\Gamma_{\rm iso}$) and base length of the tent ($L_T$) for fixed anisotropic line tension parameter ($\Gamma$) and bending rigidity ($\kappa_d$). The morphology diagrams are the intersection of surface plots from Fig. 9 with $\kappa_d = 0.1$ and $\kappa_d = 1$ planes.

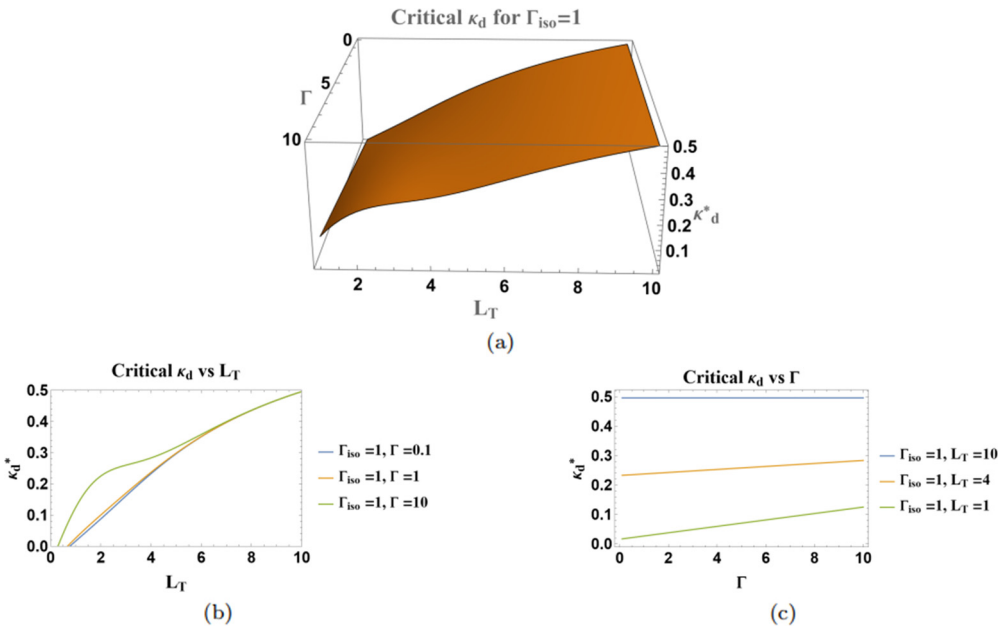


FIG. 11. Critical bending rigidity ($\kappa_d^*$) plots: Minimum value of $\kappa_d$ such that the flat sector buckles to the tent. (a) Surface plot: Critical bending rigidity ($\kappa_d^*$) as a function of $\Gamma$ and $L_T$ for $\Gamma_{\rm iso} = 1$. (b) Critical bending rigidity ($\kappa_d^*$) vs $L_T$ line plots: The intersection of the surface plot with $\Gamma$ = const. planes. (c) Critical bending rigidity ($\kappa_d^*$) vs $\Gamma$ line plots: The intersection of the surface plot with $L_T$ = const. planes.

## VII. CONCLUSIONS

Using concepts from liquid-crystal physics and topological defects, we have constructed a theoretical model to address the spontaneous formation of tentlike morphologies of PE and other polymeric lamellae. The central scheme of this model is that the sectors are formed due to trapping of a disclination in the fold field, and the tent configurations are buckled sectors. Stronger anisotropic line tension in the fold field traps a disclination more easily, and lower bending rigidity prefers the buckling of the lamellae. Within the framework of the model, we find the solution to the tent surface with the prediction of the slope formula [Eq. (23)]. We have shown that bending of a lamella involves coupling between the tilt of the polymer stems and curvature of the lamellae, which effectively reduces the bending rigidity. We hope the derived theoretical predictions on the relative stabilities of sectored morphologies of polymer lamellae will stimulate future experiments by systematically varying the key experimental parameters identified in the present model. There are several key open questions for future considerations. The chief among these is the mapping between the phenomenological parameters such as the lamellar width and their experimental realization in experiments using, for example, the extent of supercooling and solvent quality. The other key issue is that the present theory is based on conditions of thermodynamic equilibrium, whereas the crystallization phenomenon occurs under nonequilibrium conditions. The role of nonequilibrium effects in terms of conformational entropy of polymer chains that arise during crystallization on the stability of pyramids is an open question for further investigation.

## ACKNOWLEDGMENTS

We would like to thank Professor Arun Roy and Dr. Jaya Kumar Alageshan for helpful discussions. Acknowledgment is made to the National Science Foundation (Grant No. DMR 2015935).

## APPENDIX A: MONGE REPRESENTATION

We consider the parameterization of the surface in Monge representation as $\mathbf{R}\ (x, y) = \{x, y, h(x, y)\}$, where $h(x, y)$ is the height function. With this representation, we get the metric $g = 1 + (\nabla_{xy} h)^2$, where $(\nabla_{xy} h)^2 = (\partial_x h)^2 + (\partial_y h)^2$. Within the Monge approximation, i.e., $(\partial_x h)^2, (\partial_y h)^2, (\nabla_{xy} h)^2 \ll 1$, we get the spin connection:

$$A_i = \tfrac{1}{2}\epsilon_{jk}\partial_k[(\partial_i h)(\partial_j h)], \tag{A1}$$

where $\{i, j, k\} = \{x, y\}$ and antisymmetric tensor $\epsilon_{xx} = \epsilon_{yy} = 0$. The mean curvature simplifies to

$$H = \tfrac{1}{2}\nabla^2_{xy} h, \tag{A2}$$

where the flat Laplacian $\nabla^2_{xy} h = \partial^2_x h + \partial^2_y h$.

## APPENDIX B: ENERGY CALCULATIONS

### 1. Flat-sector calculations

We use a numerical approach with the transformations $x \to w\ x'$ and $y \to w\ y'$ such that the integrals become dimensionless. The free energy due to deformations

in the fold field, in units of $K_\phi$, is then given by

$$\frac{F_\phi^{(\mathrm{Sec})}}{K_\phi} = 4 \times \frac{1}{2}\Bigg[\int_0^{\zeta/\sqrt{2}} dx' \int_{-x'+\zeta/\sqrt{2}}^{-x'+L/\sqrt{2}} dy' |\partial\phi_s|^2 + \int_{\zeta/\sqrt{2}}^{L/\sqrt{2}} dx' \int_0^{-x'+L/\sqrt{2}} dy' |\partial\phi_s|^2\Bigg]. \quad \text{(B1)}$$

The factor of 4 in the expression above covers the full area of the square.

The potential energy (in $K_\phi$ units) that takes the form:

$$\frac{V_\phi^{(\mathrm{Sec})}}{K_\phi} = 4 \times \frac{1}{4}\Bigg[\int_0^{\zeta/\sqrt{2}} dx' \int_{-x'+\zeta/\sqrt{2}}^{-x'+L/\sqrt{2}} dy' \cos(4\phi_s) + \int_{\zeta/\sqrt{2}}^{L/\sqrt{2}} dx' \int_0^{-x'+L/\sqrt{2}} dy' \cos(4\phi_s)\Bigg]. \quad \text{(B2)}$$

The line tension contributions, in $K_\phi$ units, is given by

$$\frac{E_{\mathrm{iso}}^{(\mathrm{Sec})}}{K_\phi} = 4\Gamma_{\mathrm{iso}} \int_0^{L/\sqrt{2}} dx',$$

$$\frac{E_{\mathrm{an}}^{(\mathrm{Sec})}}{K_\phi} = 4\Gamma \int_0^{L/\sqrt{2}} dx' \sin^2\left[\phi_s\left(x', -x' + \frac{L}{\sqrt{2}}\right) - \frac{3\pi}{4}\right].$$

We note that the factor of 4 is for four sides of the boundary and that $\phi_b = 3\pi/4$ in the first quadrant. The total dimensionless energy of the square sector is given by

$$\mathscr{E}^{(\mathrm{Sec})} = \frac{F_\phi^{(\mathrm{Sec})}}{K_\phi} + \frac{V_\phi^{(\mathrm{Sec})}}{K_\phi} + \frac{E_{\mathrm{iso}}^{(\mathrm{Sec})}}{K_\phi} + + \frac{E_{\mathrm{an}}^{(\mathrm{Sec})}}{K_\phi} \equiv \mathscr{E}^{(\mathrm{Sec})}(\zeta, \Gamma_{\mathrm{iso}}, \Gamma, L). \quad \text{(B3)}$$

### 2. Tent calculations

The free energy due to deformations in the fold field, in units of $K_\phi$, is given by

$$\frac{F_\phi^{(\mathrm{Tent})}}{K_\phi} = 4 \times \frac{1}{2}\Bigg[\int_0^{\zeta/\sqrt{2}} dx' \int_{-x'+\zeta/\sqrt{2}}^{-x'+L_T/\sqrt{2}} \sqrt{g} dy' |\partial\phi_s|^2 + \int_{\zeta/\sqrt{2}}^{L_T/\sqrt{2}} dx' \int_0^{-x'+L_T/\sqrt{2}} \sqrt{g} dy' |\partial\phi_s|^2\Bigg],$$

where the metric $g = 1 + (\nabla h)^2 = 1 + A_w{}^2[\tanh(x')^2 + \tanh(y')^2]$. In this calculation, we ignore the coupling between curvature and fold field.

The potential and bending free energy are given by

$$\frac{V_\phi^{(\mathrm{Tent})}}{K_\phi} = 4 \times \frac{1}{4}\Bigg[\int_0^{\zeta/\sqrt{2}} dx' \int_{-x'+\zeta/\sqrt{2}}^{-x'+L_T/\sqrt{2}} dy' \sqrt{g}\cos(4\phi_s) + \int_{\zeta/\sqrt{2}}^{L_T/\sqrt{2}} dx' \int_0^{-x'+L_T/\sqrt{2}} dy' \sqrt{g}\cos(4\phi_s)\Bigg],$$

$$\frac{F_H}{K_\phi} = \frac{\kappa_d}{2} \times 4 \int_0^{L_T/\sqrt{2}} dx' \int_0^{-x'+L_T/\sqrt{2}} dy' \sqrt{g} \nabla_{xy}^2 h,$$

where dimensionless bending rigidity $\kappa_d = \kappa_{ef}/(4K_\phi)$ and mean curvature $\nabla_{xy}^2 h = -A_w[\mathrm{sech}^2(x') + \mathrm{sech}^2(y')]$.

The line tension contributions are as follows:

$$\frac{E_{\mathrm{iso}}^{(\mathrm{Tent})}}{K_\phi} = 4\Gamma_{\mathrm{iso}} \int_0^{L_T/\sqrt{2}} dx',$$

$$\frac{E_{\mathrm{an}}^{(\mathrm{Tent})}}{K_\phi} = 4\Gamma \int_0^{L_T/\sqrt{2}} dx' \sin^2\left[\phi_s\left(x', -x' + \frac{L_T}{\sqrt{2}}\right) - \frac{3\pi}{4}'\right].$$

The total free energy of the tent configuration in $K_\phi$ is given by

$$\mathscr{E}_T^{(\mathrm{Tent})} = \frac{F_\phi + V_\phi + F_H + E_{\mathrm{an}} + E_{\mathrm{iso}}}{K_\phi} \equiv \mathscr{E}_T^{(\mathrm{Tent})}(\zeta, A_w, L_T, \Gamma_{\mathrm{iso}}, \Gamma, \kappa_d). \quad \text{(B4)}$$


[1] M. Muthukumar, Shifting paradigms in polymer crystallization, in *Progress in Understanding of Polymer Crystallization*, edited by G. Reiter and G. R. Strobl (Springer, Berlin, Heidelberg, 2007), pp. 118.

[2] P. H. Geil, *Polymer Single Crystals* (Krieger Publishing Company, Malabar, 1963), Vol. 5.

[3] J. C. Wittmann and B. Lotz, Polymer decoration: The orientation of polymer folds as revealed by the crystallization of polymer vapors, J. Polym. Sci. Polym. Phys. Ed. **23**, 205 (1985).

[4] G. W. Greenwood, Molecular modelling of nucleation in polymers, Phil. Trans. R. Soc. A **361**, 539 (2003).

[5] M. Muthukumar, Modeling polymer crystallization, in *Interphases and Mesophases in Polymer Crystallization III*, edited by G. Allegra (Springer, Berlin, Heidelberg, 2005), pp. 241–274.

[6] A. Keller, A note on single crystals in polymers: Evidence for a folded chain configuration, Philos. Mag. **2**, 1171 (1957).

[7] D. Bassett, F. Frank, and A. Keller, Some new habit features in crystals of long chain compounds part IV. The fold surface geometry of monolayer polyethylene crystals and its relevance to fold packing and crystal growth, Philos. Mag. **8**, 1753 (1963).

[8] P. Geil, Nylon single crystals, J. Polym. Sci. **44**, 449 (1960).

[9] C. Garber and P. Geil, Polyoxymethylene single crystals. I. The effect of copolymer content on morphology, Makromol. Chem. **113**, 236 (1968).

[10] R. M. Briber and F. Khoury, The morphology of poly (vinylidene fluoride) crystallized from blends of poly (vinylidene fluoride) and poly (ethyl acrylate), J. Polym. Sci. B Polym. Phys. **31**, 1253 (1993).

[11] A. Toda, M. Okamura, M. Hikosaka, and Y. Nakagawa, AFM observation of polyethylene single crystals: Selective handedness of screw dislocations in a chair type, Polymer **44**, 6135 (2003),.

[12] J. K. Alageshan, Y. Hatwalne, and M. Muthukumar, Stability of the sectored morphology of polymer crystallites, Phys. Rev. E **94**, 032506 (2016).
[13] H. S. Seung and D. R. Nelson, Defects in flexible membranes with crystalline order, Phys. Rev. A **38**, 1005 (1988).
[14] M. W. Deem and D. R. Nelson, Free energies of isolated five- and seven fold disclinations in hexatic membranes, Phys. Rev. E **53**, 2551 (1996).
[15] L. D. Landau and E. M. Lifshitz, *Theory of Elasticity* (Elsevier, Oxford, 1986).
[16] P. M. Chaikin and T. C. Lubensky, *Principles of Condensed Matter Physics* (Cambridge University Press, Cambridge, 1995).
[17] T. C. Lubensky, and F. C. MacKintosh, Theory of "ripple" phases of lipid bilayers, Phys. Rev. Lett. **71**, 1565 (1993).
[18] C. M. Chen, T. C. Lubensky, and F. C. MacKintosh, Phase transitions and modulated phases in lipid bilayers, Phys. Rev. E **51**, 504 (1995).
[19] V. Vitelli and D. R. Nelson, Phys. Rev. E **74**, 021711 (2006).
[20] D. R. Nelson, Toward a tetravalent chemistry of colloids, Nano Lett. **2**, 1125 (2002).
[21] D. Nelson and L. Peliti, Fluctuations in membranes with crystalline and hexatic order, J. Phys. **48**, 1085 (1987).
[22] D. R. Nelson and B. Halperin, Solid and fluid phases in smectic layers with tilted molecules, Phys. Rev. B **21**, 5312 (1980).
[23] M. Warner and E. Terentjev, *Liquid Crystal Elastomers* (Oxford University Press, Oxford, 2003), Vol. 120.
[24] M. Bowick and L. Giomi, Two-dimensional matter: Order, curvature and defects, Adv. Phys. **58**, 449 (2008).
[25] W. Helfrich, Elastic properties of lipid bilayers: Theory and possible experiments, Z. Naturforschung C **28**, 693 (1973).
[26] A. Rapini and M. Papoular, Distorsion d'une lamelle nématique sous champ magnétique conditions d'ancrage aux parois, J. Phys. Colloques **30**, C4 (1969).